An Identification Procedure for Rate-Dependency of Friction in Robotic Joints with Limited Motion Ranges☆

Masayoshi Iwatani and Ryo Kikuuwe

Department of Mechanical Engineering
Kyushu University
744 Motooka, Nishi-ku, Fukuoka 819-0395, Japan
E-mail: {iwatani@ctrl., kikuuwe@}mech.kyushu-u.ac.jp

Abstract

This paper proposes a procedure for identifying rate-dependent friction of robotic manipulators of which the motion is limited due to the configuration or the environment. The procedure is characterized by the following three features: (i) the rate dependency is represented by line sections connecting sampled velocity-force pairs, (ii) the robot is position-controlled to track desired trajectories that are some cycles of sinusoidal motion with different frequencies, and (iii) each velocity-force pair is sampled from one cycle of the motion with subtracting the effects of the gravity and the inertia. The procedure was validated with a six-axis industrial robotic manipulator YASKAWA MOTOMAN-HP3J, of which the joints are equipped with harmonic-drive transmissions of the reduction ratios of 81.5 to 224. The experimental results show that the identification is achieved with a sufficient accuracy with the 20 degrees of motion of each joint. In addition, the results were utilized for friction compensation, successfully reducing the effect of the friction by 60 to 80 percent.

Keywords: Rate-dependent friction, Identification, Compensation, Robotic manipulator

1. Introduction

For the control of robotic manipulators, friction in the joints is one of major disturbances that degrade the accuracy and the precision of control. One straightforward idea to deal with this problem is to calibrate the friction properties of the robot in advance and to compensate the friction force by producing the actuator forces that cancel the friction forces. It is however usually difficult

☆The paper extends the authors' previous conference paper [1] by including new experimental results.

to find appropriate models of the friction phenomena and, even if an appropriate model is available, it is also difficult to clarify how the values of the parameters should be chosen.

Many friction models have been proposed so far, and they vary in the treatment of the discontinuity around the zero velocity and the microscopic elastic displacement in the static friction. A common point shared by various friction models is that they employ a user-defined function of velocity that represents the rate-dependent friction law. That is, for any kinds of friction models, the magnitude of the friction force as a function of the velocity must be identified experimentally.

Experimental identification of the rate dependency of the friction force is not always an easy task. Problems such as the limited motion range and the effects of the gravity and the inertia make the identification complicated. The motion of an assembled robotic manipulator is generally limited by the configuration or the environment. Appropriate procedures are needed to measure the friction force at high velocities in a limited motion range, and the identification results need to be insensitive to the effects of inertia and gravity.

This paper presents a systematic procedure to identify the velocity-friction force relation of devices with limited motion range. The procedure was validated with an industrial six-joint manipulator YASKAWA MOTOMAN-HP3J. It is shown that the identification with a sufficient accuracy was achieved with 20 degrees of motion of the joints. This paper also shows the application of identified results to friction compensation.

The remainder of this paper is organized as follows: Section 2 overviews previous studies on identification of rate-dependent friction. Section 3 proposes the new procedure. Section 4 and 5 show experimental results obtained with a six-axis manipulator. Section 6 provides concluding remarks.

2. Related Work

Many friction models have been proposed for the purpose of control. They have realized friction property such as rate-dependency in the kinetic friction [2], elastic displacement in the static friction [3], hysteresis in the velocity-friction relation, stick slip motion [4], non-drifting [5][6], and smoothness of the output force [7]. Discrete-time models have also been considered [8][9]. There have been applications of the models to friction compensation [5][10], and harmonic drive transmissions especially have been the target of applications of modeling studies [11][12][13]. One common feature shared by many models including dynamic friction models is that they employ functions of velocity for representing the rate-dependent friction force in the kinetic friction region. It means that the velocity-friction relation must be calibrated in advance for using any kinds of existing models including dynamic friction models.

Rate-dependent friction of manipulators can be identified by maintaining a constant velocity for a certain period of time [10][14]. In such methods, constant velocity commands are sent to the devices, and the resultant actuator torque

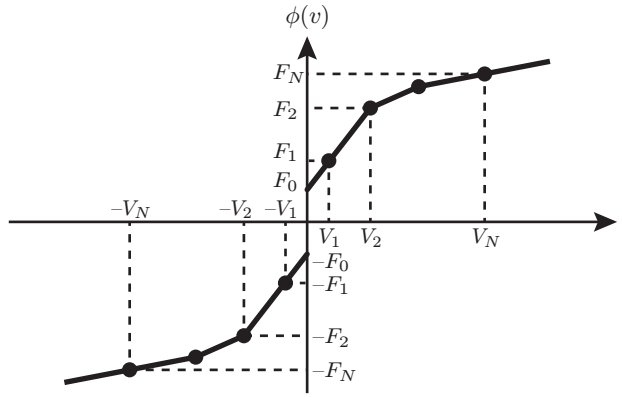

Figure 1: Fitted curve $\phi(v)$ defined by (8)

to maintain the velocity is observed. One drawback of such methods is that maintaining high velocity is generally difficult within a limited range of motion.

Another kind of approach is to apply sinusoidal or saw-tooth torque signals to devices to be identified [15][16]. Such torque command, resulting reciprocating motion, requires a certain level of carefulness in choosing the torque amplitudes so that the trajectory of motion is bounded to a limited range.

The gravity and the inertia affect the accuracy of the identified results. A straightforward idea to deal with these factors is to incorporate a system model including the gravity and the inertia into the identification procedure [10][15][16][17]. Major drawbacks of this approach are that the identification of the system model is usually a hard task, and that the identification accuracy of the friction depends on the accuracy of the whole system model.

3. Procedure

3.1. Overview

This section describes a new identification procedure for rate-dependent friction laws. The procedure is to obtain a set of N velocity-force pairs

$$\mathcal{S} \triangleq \{[V_1, F_1], \cdots, [V_N, F_N]\}, \tag{1}$$

which describes the relation between the velocity and the friction force as shown in Figure 1. The joint to be identified is controlled to follow sinusoidal trajectories with N different frequencies with a high-gain PID position controller. One cycle of motion is performed for each frequency. The pair $[V_n, F_n]$ is chosen so that the effects of inertia and gravity are small. The identification on each joint is performed on a one-by-one basis, with the other joints being locked by local position controllers.

3.2. Details

The input to the procedure is the following three parameters:

- V : The maximum desired velocity
- A : The amplitude of the sinusoidal motion
- N : The number of sampled velocities

The maximum velocity V should be chosen so that it includes the range of velocity in which the friction force should be identified. The amplitude A should be chosen small enough to match the hardware limitation, and should be smaller to save the time needed for the identification procedure. Its lower bound is determined by the capacity of the actuator because, with a fixed V value, the desired acceleration command is inversely proportional to the A value, as will be shown later. The number N of sampled velocities should be chosen considering the trade-off between the precision of the fitted curve and the time needed for the identification.

The desired trajectory for the identification of the set $\mathcal{S}$ is generated as the following function of the time t:

$$p_d(t) \triangleq \frac{A}{2}\left(1 - \cos\left(\frac{2\nu(t)V}{AN}(t - T_{\nu(t)})\right)\right) \tag{2}$$

where

$$T_n \triangleq \sum_{j=1}^{n-1} \frac{\pi AN}{jV} \tag{3a}$$

$$\nu(t) \triangleq n \text{ s.t. } t \in \mathcal{T}_n \triangleq [T_n, T_{n+1}). \tag{3b}$$

This position trajectory $p_d(t)$ is based on the following velocity trajectory:

$$v_d(t) \triangleq \frac{\nu(t)V}{N} \sin\left(\frac{2\nu(t)V}{AN}(t - T_{\nu(t)})\right). \tag{4}$$

These trajectories $p_d(t)$ and $v_d(t)$ are illustrated in Figure 2. Here, it can be seen that $p_d(t)$ is composed of N times of sinusoidal movements with N different frequencies. The amplitude of the desired position p_d is fixed to A, and the maximum velocity of the nth cycle is nV/N. It should be noted that the amplitude of $\dot{v}_d$ is proportional to V^2/A, and thus the choice of the A value is lower-bounded by the capacity of the actuator.

Once the joint is position-controlled to track the aforementioned desired trajectory, the data as shown in Figure 3 is expected to be obtained. Here, it is advisable that the gains of the position controller should be set as high as possible. The control accuracy however only needs to be enough to realize the velocity above the maximum desired velocity V, which is given as a parameter of the procedure. This is because what is important here is the relation between the

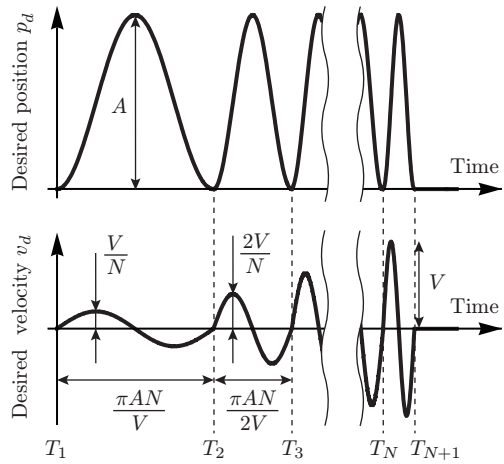

Figure 2: Desired trajectory $p_d(t)$ and its derivative $v_d(t)$ for the proposed identification procedure

applied force f and the actual velocity v, which describes the physical property of the joint, and is not the relation between v and the desired velocity v_d. With a sampling interval Δt, the measured velocity v_i and the applied force f_i are obtained at the time t_i where $i \in \{1, \cdots, I\}$ and

$$I \triangleq T_{N+1}/(\Delta t). \tag{5}$$

Consequently, an experiment in the presented procedure provides the following sets of data:

$$\begin{aligned} \mathcal{T}_{\text{all}} &= \{t_1, t_2, \cdots, t_I\} \\ \mathcal{V}_{\text{all}} &= \{v_1, v_2, \cdots, v_I\} \\ \mathcal{F}_{\text{all}} &= \{f_1, f_2, \cdots, f_I\}. \end{aligned} \tag{6}$$

The data $\{\mathcal{T}_{\text{all}}, \mathcal{V}_{\text{all}}, \mathcal{F}_{\text{all}}\}$ can be utilized to obtain the set $\mathcal{S}$ through the following function:

$$\text{FunctionA}(\mathcal{T}_{\text{all}}, \mathcal{V}_{\text{all}}, \mathcal{F}_{\text{all}}) \tag{7a}$$
$$\text{for } n := 1 \text{ to } N \tag{7b}$$
$$\mathcal{V}_n := \{v_i \in \mathcal{V}_{\text{all}} \mid t_i \in \mathcal{T}_n \wedge v_i \geq cnV/N\} \tag{7c}$$
$$\mathcal{F}_n^+ := \{f_i \in \mathcal{F}_{\text{all}} \mid t_i \in \mathcal{T}_n \wedge v_i \geq cnV/N\} \tag{7d}$$
$$\mathcal{F}_n^- := \{f_i \in \mathcal{F}_{\text{all}} \mid t_i \in \mathcal{T}_n \wedge v_i \leq -cnV/N\} \tag{7e}$$
$$V_n := \text{Average}(\mathcal{V}_n) \tag{7f}$$
$$F_{sn}^+ := \text{Average}(\mathcal{F}_n^+) \tag{7g}$$
$$F_{sn}^- := \text{Average}(\mathcal{F}_n^-) \tag{7h}$$
$$F_n := (F_{sn}^+ - F_{sn}^-)/2 \tag{7i}$$

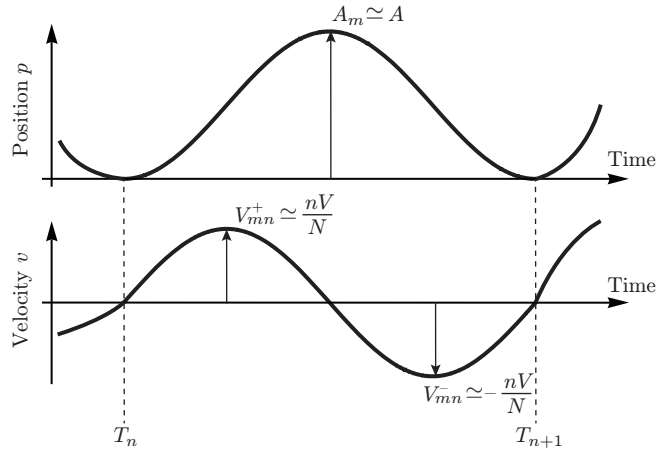

(a) One part of waveform of position p and velocity v

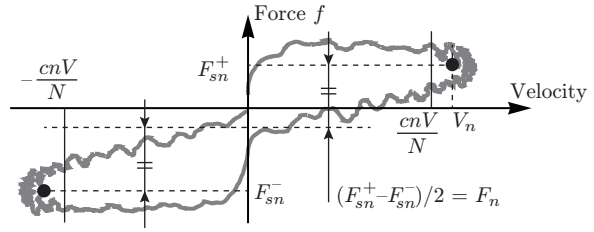

(b) Relation between velocity v and force f

Figure 3: Schematic illustration of data that could be obtained from the procedure

$$\text{end for} \tag{7j}$$

$$\mathcal{S} := \{[V_1, F_1], \cdots, [V_N, F_N]\} \tag{7k}$$

$$\text{Return } \mathcal{S}. \tag{7l}$$

Figure 3(b) illustrates the relations among some variables that appear in this procedure. Here, Average($\mathcal{X}$) is a function that returns the average value of the elements of input set $\mathcal{X}$. The ratio $c \in [0, 1)$ determines the boundaries of the range of the sampled data used for the identification, by multiplying the maximum desired velocity nV/N in each cycle as can be seen in (7c)-(7e) and Figure 3. The ratio is set at $c = 0.8$ in this paper.

Now, the set $\mathcal{S}$ is obtained through algorithm (7). Based on the set $\mathcal{S}$, the rate-dependent friction is defined as the following function $\phi(v)$:

$$f = \phi(v) \triangleq \text{sgn}(v)\big(B_{n(v)}(|v| - V_{n(v)}) + F_{n(v)}\big) \tag{8}$$

where

$$B_n \triangleq (F_{n+1}-F_n)/(V_{n+1}-V_n) \ (n \in \{1, \cdots, N-1\}) \tag{9a}$$

$$B_0 \triangleq B_1 \tag{9b}$$

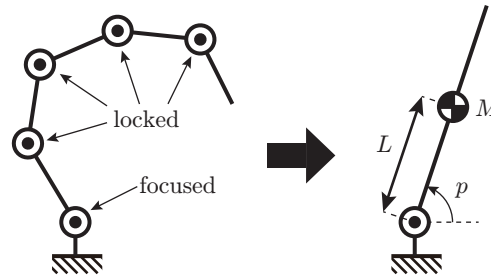

Figure 4: Schematic illustration of robot regarded as a 1-link manipulator

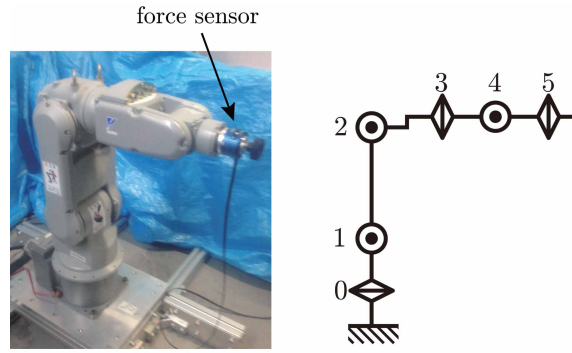

(a) MOTOMAN-HP3J (b) Configuration

Figure 5: Experimental setup

$$B_N \triangleq B_{N-1} \tag{9c}$$

$$V_0 \triangleq 0 \tag{9d}$$

$$V_{N+1} \triangleq +\infty \tag{9e}$$

$$F_0 \triangleq F_1 - B_0 V_1 \tag{9f}$$

$$n(v) \triangleq n \text{ s.t. } V_n \leq v < V_{n+1}. \tag{9g}$$

The function is illustrated in Figure 1. It is a combination of line sections connecting the elements of the set $\mathcal{S}$, and is symmetric with respect to $v = 0$. Note that all parameters $\{B_n, V_n, F_n\}$ are derived from the set $\mathcal{S}$.

3.3. Analysis on the influence of inertia and gravity

The algorithm in this paper uses only the data near the velocity peaks, and estimates the friction force by taking the semi-amplitude of the force values at the velocity peaks. This is based on the intention to minimize the effects of the inertia and the gravity to the estimated friction force F_n as explained by the following.

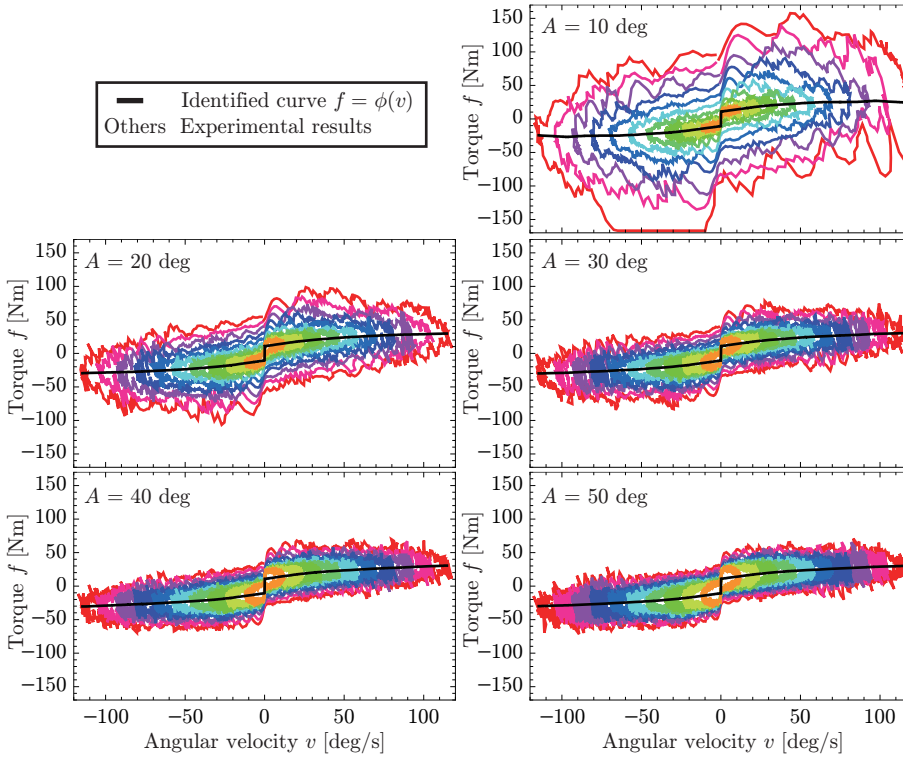

Figure 6: Experimental results and the identified curves in the cases of various A at Joint 1. Experimental results are unbiased.

Let us regard the robot as a 1-link rotational manipulator because the joints except the focused one are locked as shown in Figure 4. Then, the actuator force f can be represented as follows:

$$f = f_f(\dot{p}) + I\ddot{p} + MLg\cos(p) \tag{10}$$

where $f_f(v)$ is the rate-dependent friction force, I is the moment of inertia around the joint, M is the total mass, L is the length from the joint to the center of mass (COM), p is the angle between the horizontal surface and the line passing through the joint and the COM, and g is the gravity acceleration.

As has been explained in Section 3.2, the angle p can be given as a sinusoidal function of time t as follows:

$$p = p_0 + A\cos(\omega t) \tag{11}$$

where A and ω are the amplitude and the angular frequency of the motion and p_0 is a constant, respectively. Then, (10) can be rewritten as follows:

$$f = f_f\left(A\omega\sin(\omega t)\right) - IA\omega^2\cos(\omega t) + MLg\cos\left(p_0 + A\cos(\omega t)\right) \tag{12}$$

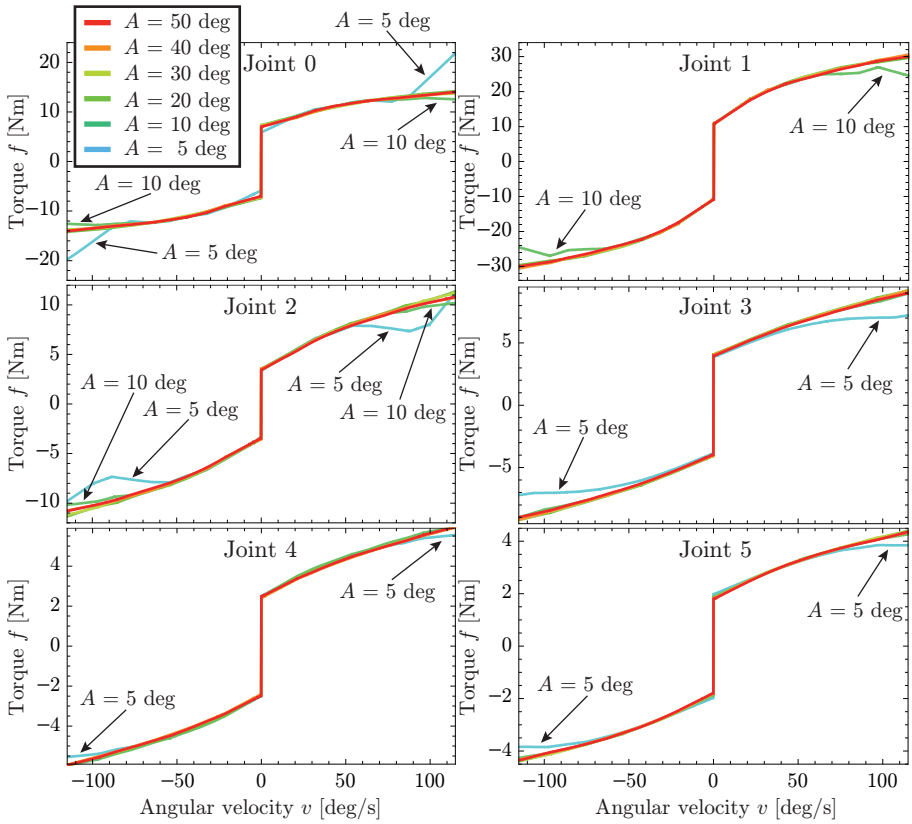

Figure 7: Identification results of each joint in various cases of A under $V = 115$ deg/s (2.0 rad/s) and $N = 10$. The result in the case of $A = 5$ deg at Joint 1 was not obtained due to the limit of the servo controller.

The force values F_{sn}^{+} and F_{sn}^{-} at the velocity peaks can be written by (12) with $t = \pi/(2\omega)$ and $3\pi/(2\omega)$ as follows:

$$F_{sn}^{+} = f_f(A\omega) + MLg\cos(p_0) \tag{13a}$$
$$F_{sn}^{-} = f_f(-A\omega) + MLg\cos(p_0) \tag{13b}$$

Substituting (13a) and (13b) for (7i) yields the following equation:

$$F_n = \left(f_f(A\omega) - f_f(-A\omega)\right)/2 \simeq f_f(A\omega) \tag{14}$$

because of the assumption that the rate-dependent friction force is symmetric with respect to $v = 0$, that is, $f_f(-A\omega) \simeq -f_f(A\omega)$.

What (14) implies is that F_n does not depend on the inertia term $I\ddot{p}$ or the gravity term $MLg\cos(p_0)$. This can be explained by the fact that the acceleration is close to zero at the velocity peaks and the angle joint at the two velocity peaks are close to each other.

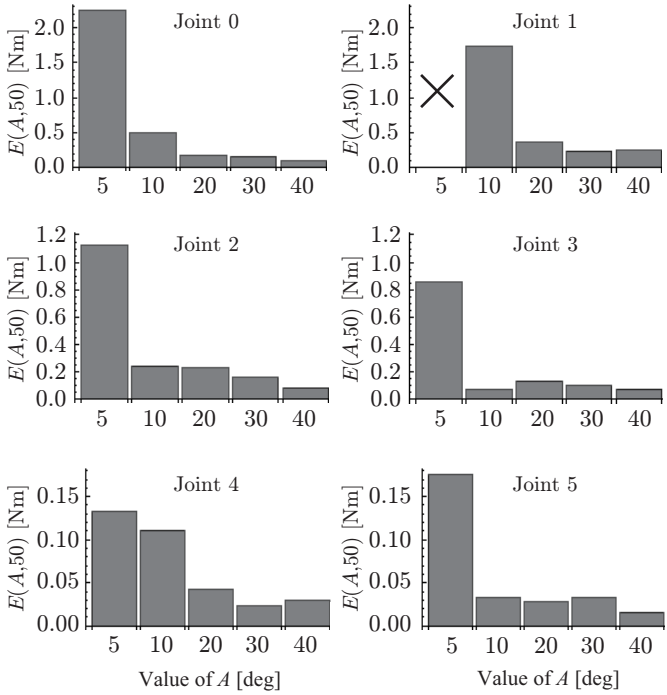

Figure 8: Difference between each curve and the curve of $A = 50$ deg based on (15) under $V = 115$ deg/s (2.0 rad/s) and $N = 10$. The symbol $\times$ means that the result was not obtained due to the limit of the servo controller.

4. Experiment: Identification

4.1. Experimental setup

The proposed identification procedure was experimentally tested with a six-axis robotic manipulator YASKAWA MOTOMAN-HP3J shown in Figure 5. A harmonic drive transmission is embedded to each joint. Table 1 shows the specification of each joint. A force sensor NITTA IFS-50M31A25-I25 is attached at the end-effector to measure the external force in experiments of friction compensation to which the identified results are applied.

This paper does not include the experimental comparison with methods in the literature. The proposed method is based on the position control, which is intrinsically capable of limiting the joint motion within the mechanical limitations. In contrast, other methods are based on torque command [15][16] or velocity command [10][14][17], and thus there is the possibility that the motion of the joint arrives in the mechanical limitation. Therefore, experiments under the same condition cannot be performed. Previous methods focused on, for example, identification in low velocity range [10], position-dependent friction [14], dynamic friction models [15], nonlinear optimization problem [16], or identification using transfer functions [17].

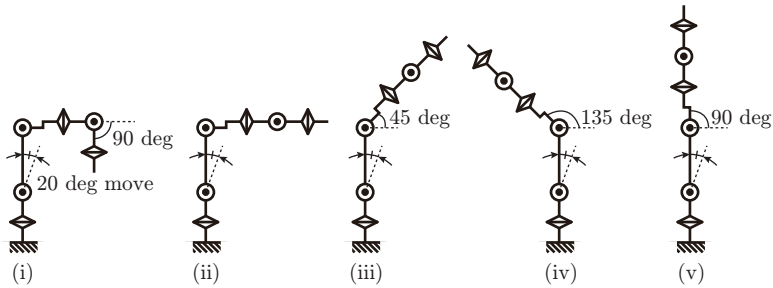

(a) Conditions of the posture

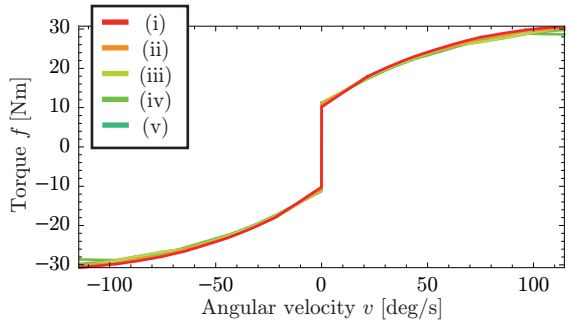

(b) Identified curves

Figure 9: Identification results with various postures of Joint 1 under the condition of $A = 20$ deg, $V = 115$ deg/s (2.0 rad/s) and $N = 10$. The effect of inertia is largest in Posture (v) and smallest in Poster (i). The effect of gravity is largest in Posture (ii) and smallest in (v).

4.2. Sensitivity to the choice of A

It is desirable to set A as small as possible for reducing the time needed for the identification. Figure 6 shows experimental results and identified curves with various values of A, under $V = 115$ deg/s (2.0 rad/s) and $N = 10$. Figure 6 is the result of Joint 1, where the effect of the gravity and the inertia is the largest among all joints. The bias of each experimental result is removed to make it comparable to the fitted curve $\phi(v)$ obtained by the proposed procedure. It can be seen that smaller A, resulting larger effect of inertia, broadens the width of the curves and also perturbs the fitted curve $\phi(v)$. Therefore, it can be concluded that too small A deteriorates the accuracy of the identification. The following shows how small A can be at each joint.

Table 1: Specification of the experimental setup

Joint number [-]	0	1	2	3	4	5
Reduction ratio [-]	100	224	120	120	100	81.5
Maximum velocity [deg/s]	200	135	190	250	300	360
Maximum torque [Nm]	95.1	213.1	114.1	34.2	28.5	23.3

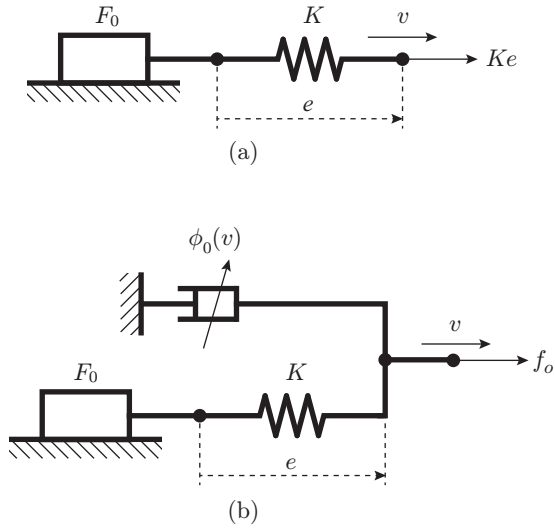

Figure 10: Friction models for compensation: (a) the model in [18], (b) the model in this paper

Figure 7 is the identified results with various A at each joint. In this figure, one can see that the curves of A larger than 10 deg are almost overlapping. Thus, it can be said that the amplitude of trajectory $A = 20$ deg is enough to identify the friction curve appropriately. Moreover, it is clear that the slope of the identified curves in the high velocity range is different from that in low velocity range. This indicates that the high velocity range should also be identified experimentally, not only by extrapolation.

In order to validate the results quantitatively, we use the following distance metric:

$$E(A_1, A_2) = \sqrt{\frac{1}{V}\int_0^V (\phi_{A_1}(v) - \phi_{A_2}(v))^2 dv}. \tag{15}$$

This metric represents the difference between the curves $\phi_{A_1}(v)$ and $\phi_{A_2}(v)$ that are obtained with $A = A_1$ and A_2 respectively. Figure 8 shows the quantitative difference between each curve and the curve of $A = 50$ deg at each joint. It is shown that the differences are large when $A = 5$ or 10 deg. These results correspond to Figure 7, quantitatively indicating that the trajectory amplitude of $A = 10$ or 20 deg is the minimum necessary value for appropriate identification, under the condition of the range of velocity $V = 115$ deg/s (2.0 rad/s) in the device MOTOMAN-HP3J.

4.3. Sensitivity to the posture

Another set of experiments were carried out to show the effects of inertia and gravity on the identification results. The identification was performed on Joint 1 with five different postures shown in Figure 9(a) under the condition of $A = 20$ deg, $V = 115$ deg/s (2.0 rad/s) and $N = 10$. The different postures yield the different inertia and gravity force with respect to the joint. Figure 9(b) is the identification results, which show that the curves are almost overlapping. Therefore, It can be said that the dependency of identification results on the posture is small. This indicates that using only the data near the velocity peaks (lines (7c)-(7e)), and taking the semi-amplitude of the force (line (7i)) are effective enough to remove the effects of the inertia and the gravity.

5. Experiment: Friction Compensation

The identified results were validated through experiments of friction compensation. Here, the identified curve is combined with a dynamic friction model of Hayward and Armstrong [8] and employed for friction compensation in the similar manner as the method presented by Marvash and Okamura [18]. In the technique presented in [18], the friction force is modeled as a serial connection of a spring and a Coulomb friction element, as illustrated in Figure 10(a). In the same light, we used a model illustrated in Figure 10(b), in which a nonlinear viscosity is connected in parallel with a Coulomb friction-spring element. The model in Fig. 10(b) can be described as follows:

$$Ke \in F_0 \mathrm{sgn}(v - \dot{e}) \tag{16a}$$

$$f_o = Ke + \phi_0(v) \tag{16b}$$

where

$$\phi_0(v) \triangleq \phi(v) - F_0 \mathrm{sgn}(v). \tag{17}$$

Here, e is the displacement of the spring, and (16a) represents the fact that the Coulomb friction force $F_0\mathrm{sgn}(v - \dot{e})$ balances the spring force Ke. By noting the relation between $\phi(v)$ and F_0 illustrated in Figure 1, we can easily see that $\phi_0(v)$ is a continuous function. The K value was chosen as 175 Nm/deg (10000 Nm/rad) through preliminary experiments. Higher K values resulted in oscillation and lower K values resulted in insufficient compensation.

By using the backward Euler method, (16a) is discretized as follows:

$$Ke_k \in F_0 \mathrm{sgn}\left(v_k - \frac{e_k - e_{k-1}}{\Delta t}\right) \tag{18}$$

where k denotes the discrete-time index, Δt is the sampling interval, and $\mathrm{sgn}(x)$ is the set-valued function defined as follows:

$$\mathrm{sgn}(x) \triangleq \begin{cases} x/|x| & \text{if } |x| \neq 0 \\ [-1, 1] & \text{if } |x| = 0. \end{cases} \tag{19}$$

Through careful derivation, one can see that (18) can be solved with respect to e_k, and the solution is

$$e_k = \frac{F_0}{K}\mathrm{sat}\left(\frac{K}{F_0}\left(\Delta t v_k + e_{k-1}\right)\right) \tag{20}$$

where

$$\mathrm{sat}(x) \triangleq \begin{cases} x/|x| & \text{if } |x| > 1 \\ x & \text{if } |x| \leq 1. \end{cases} \tag{21}$$

This derivation can be done by using the relation

$$y \in \mathrm{sgn}(x - y) \iff y = \mathrm{sat}(x),\ \forall x, y \in \mathbb{R}, \tag{22}$$

of which the proof is provided in [19]. Another important point is that, in order to ensure the stability, the actuator force f_c used for the friction compensation should be slightly smaller than the actual friction force. Thus, the actuator force f_c should be determined as follows:

$$f_c = Rf_o \tag{23}$$

where R is an appropriate positive constant that is slightly smaller than 1. We used $R = 0.9$ in the experiments reported in this paper.

In conclusion, a discrete-time algorithm to obtain the actuator force $f_{c,k}$ for friction compensation is obtained as follows:

$$e_k := \frac{F_0}{K}\mathrm{sat}\left(\frac{K}{F_0}\left(\Delta t v_k + e_{k-1}\right)\right) \tag{24a}$$

$$f_{o,k} := Ke_k + \phi_0(v_k) \tag{24b}$$

$$f_{c,k} := Rf_{o,k}. \tag{24c}$$

The algorithm (24) exemplifies the combined application of the identified curve $\phi_0(v_k)$ and dynamic friction models.

5.1. Manual moving

In this experiment, the experimenter grasped the end-effector of the manipulator and moved it cyclically in both cases without friction compensation and with compensation. The external torque f_s to move the manipulator was derived from the output values of the force sensor attached at the end-effector and the length of the moment arm. All joints except the focused joint were locked by local position controller with as high gain as possible. Gravity compensation, of which the parameters were calibrated in advance, was applied to each joint. The experimenter intended to move the end-effector by hand at the frequency of 0.5 Hz, being paced by a metronome.

Figure 11 shows the experimental results of friction compensation. Data of the Joint 3 and 5 were not obtained due to the limitation of the force sensor, of which the rated torque is smaller than the necessary torque to move these joints.

Figure 11 shows that, while the velocity v does not exhibit significant difference between the two cases, the measured torque f does exhibit distinct difference, which are the lowered magnitudes and the forward-shifted phase in the case with the compensation. Such features cannot be created by the experimenter's intention and can be solely attributed to the reduction of the friction force due to the friction compensation. One can infer that the phase shift is also a consequence of the reduction of the friction force, which results in the inertia being dominant.

The measured velocity and the measured external torque were evaluated quantitatively by using the following criteria:

$$V_s = \sqrt{\frac{1}{T_e}\int_0^{T_e} v_s^2 \, dt}, \quad F_s = \sqrt{\frac{1}{T_e}\int_0^{T_e} f_s^2 \, dt} \tag{25}$$

where T_e is the time period of an experiment. The results are shown in Fig 12. This figure shows that, although the magnitude of the measured velocity is almost equal between the two cases, the magnitude of the measured torque is smaller by 60 to 80 percent in the case with the friction compensation. It means that the friction compensation decreases the magnitude of torque required to realize given velocities. These results indicate that the function identified by the proposed procedure is effective in the friction compensation.

5.2. Feedback position tracking

In this experiment, a low-gain PD position controller for a saw-teeth desired trajectory was applied to each joint one-by-one in the four cases as follows: no compensation (NC), compensation by the model of Mahvash and Okamura [18] (MO), MO and linear viscosity compensation (MOL), MO and compensation using functions identified by the proposed procedure (MOP). As is the case with Section 5.1, all joints except the focused one were locked and the gravity compensation was applied to each joint. In the case of MO, the following equation was used in stead of (24b):

$$f_{o,k} := Ke_k \tag{26}$$

and in the case of MOL, the following equation was used:

$$f_{o,k} := Ke_k + B_c v_k \tag{27}$$

where B_c is a constant coefficient for the linear viscosity compensation.

Figure 13 shows the results, which show that the tracking accuracy is overall highest with MOP. Figure 14 shows a quantitative comparison of the tracking errors with the following criterion:

$$E_s = \sqrt{\frac{1}{T_e}\int_0^{T_e} (p_d - p_s)^2 \, dt}. \tag{28}$$

Figure 14 also shows that MOP provides smaller tracking error than MOL, MO, and NC. These results indicates that the friction compensation significantly reduces the tracking error of position control, and also indicates that using the rate-dependent friction law, which is obtained by the proposed method, is more effective than simple Coulomb friction law or Coulomb plus linear viscous friction law. The results also supports the validity of the method combining the identified curve and dynamic friction models.

6. Conclusion

This paper has presented an identification procedure for rate-dependent friction of manipulators of which the motion is limited. The procedure has the following characteristic features: (i) the function representing the rate dependency is defined by line sections connecting sampled velocity-force pairs, (ii) each joint is controlled as it tracks desired position trajectories consisting of some cycles of sinusoidal motion with different frequencies, and (iii) each velocity-force pair is sampled from each cycle of the motion with subtracting the effects of the gravity and the inertia. The procedure was applied to a YASKAWA MOTOMAN-HP3J, which is a six-joint robotic manipulator with harmonic-drive transmissions. It has been shown that the identification up to the velocity of 115 deg/s (2.0 rad/s) was achieved with a 20-deg sinusoidal motion. Experimental results have also shown that the friction of the manipulator was reduced by 60 to 80 percent by the compensation using the identified function.

References

[1] M. Iwatani, R. Kikuuwe, An identification procedure for rate-dependent friction laws of robotic manipulator with limited motion range, Proceedings of the 10th Asian Control Conference 2015 (2015) 526–530.

[2] B. Armstrong-Hélouvry, P. Dupont, C. Canudas de Wit, A survey of models, analysis tools and compensation methods for the control of machines with friction, Automatica 30 (7) (1994) 1083–1138.

[3] P. R. Dahl, A solid friction model, Tech. Rep. TOR-0158(3107-18)-1, Aerospace Corporation (1968).

[4] C. Canudas de Wit, H. Olsson, K. J. Åström, P. Lischinsky, A new model for control of systems with friction, IEEE Transactions on Automatic Control 40 (3) (1995) 419–425.

[5] J. Swevers, F. Al-Bender, C. G. Ganseman, T. Prajogo, An integrated friction model structure with improved presliding behavior for accurate friction compensation, IEEE Transactions on Automatic Control 45 (4) (2000) 675–686.

[6] F. Al-Bender, V. Lampaert, J. Swevers, The generalized Maxwell-slip model: a novel model for friction simulation and compensation, IEEE Transactions on Automatic Control 50 (11) (2005) 1883–1887.

[7] X. Xiong, R. Kikuuwe, M. Yamamoto, A multistate friction model described by continuous differential equations, Tribology Letters 51 (3) (2013) 513–523.

[8] V. Hayward, B. Armstrong, A new computational model of friction applied to haptic rendering, in: P. Corke, J. Trevelyan (Eds.), Experimental Robotics VI, Vol. 250 of Lecture Notes in Control and Information Sciences, Springer-Verlag, 2000, pp. 404–412.

[9] R. Kikuuwe, N. Takesue, A. Sano, H. Mochiyama, H. Fujimoto, Admittance and impedance representations of friction based on implicit Euler integration, IEEE Transactions on Robotics 22 (6) (2006) 1176–1188.

[10] C. W. Kennedy, J. P. Desai, Modeling and control of the Mitsubishi PA-10 robot arm harmonic drive system, IEEE/ASME Transactions on Mechatronics 10 (3) (2005) 263–274.

[11] T. Tjahjowidodo, F. Al-Bender, H. Van Brussel, W. Symens, Friction characterization and compensation in electro-mechanical systems, Journal of Sound and Vibration 308 (3) (2007) 632–646.

[12] M. Iwatani, R. Kikuuwe, M. Yamamoto, Friction compensation of harmonic drive gearing based on parallel viscoelasto-plastic friction model, Journal of Robotics Society of Japan 32 (5) (2014) 445–455 (in Japanese).

[13] M. T. S. Aung, R. Kikuuwe, M. Yamamoto, Friction compensation of geared actuators with high presliding stiffness, Transactions of ASME: Journal of Dynamic Systems, Measurement, and Control 137 (1) (2015) 011007.

[14] E. Garcia, P. Gonzalez de Santos, C. Canudas de Wit, Velocity dependence in the cyclic friction arising with gears, The International Journal of Robotics Research 21 (9) (2002) 761–771.

[15] M. R. Kermani, R. V. Patel, M. Moallem, Friction identification and compensation in robotic manipulators, IEEE Transactions on Instrumentation and Measurement 56 (6) (2007) 2346–2353.

[16] M. Vakil, R. Fotouhi, P. N. Nikiforuk, Energy-based approach for friction identification of robotic joints, Mechatronics 21 (3) (2011) 614–624.

[17] X. Chen, F. Fang, X. Luo, A friction identification approach based on dual-relay feedback configuration with application to an inertially stabilized platform, IEEE Transactions on Automatic Control 40 (3) (1995) 419–425.

[18] M. Mahvash, A. M. Okamura, Friction compensation for enhancing transparency of a teleoperator with compliant transmission, IEEE Transactions on Robotics 23 (6) (2007) 1240–1246.

[19] R. Kikuuwe, N. Takesue, H. Fujimoto, A control framework to generate nonenergy-storing virtual fixtures: Use of simulated plasticity, IEEE Transactions on Robotics 24 (4) (2008) 781–793.

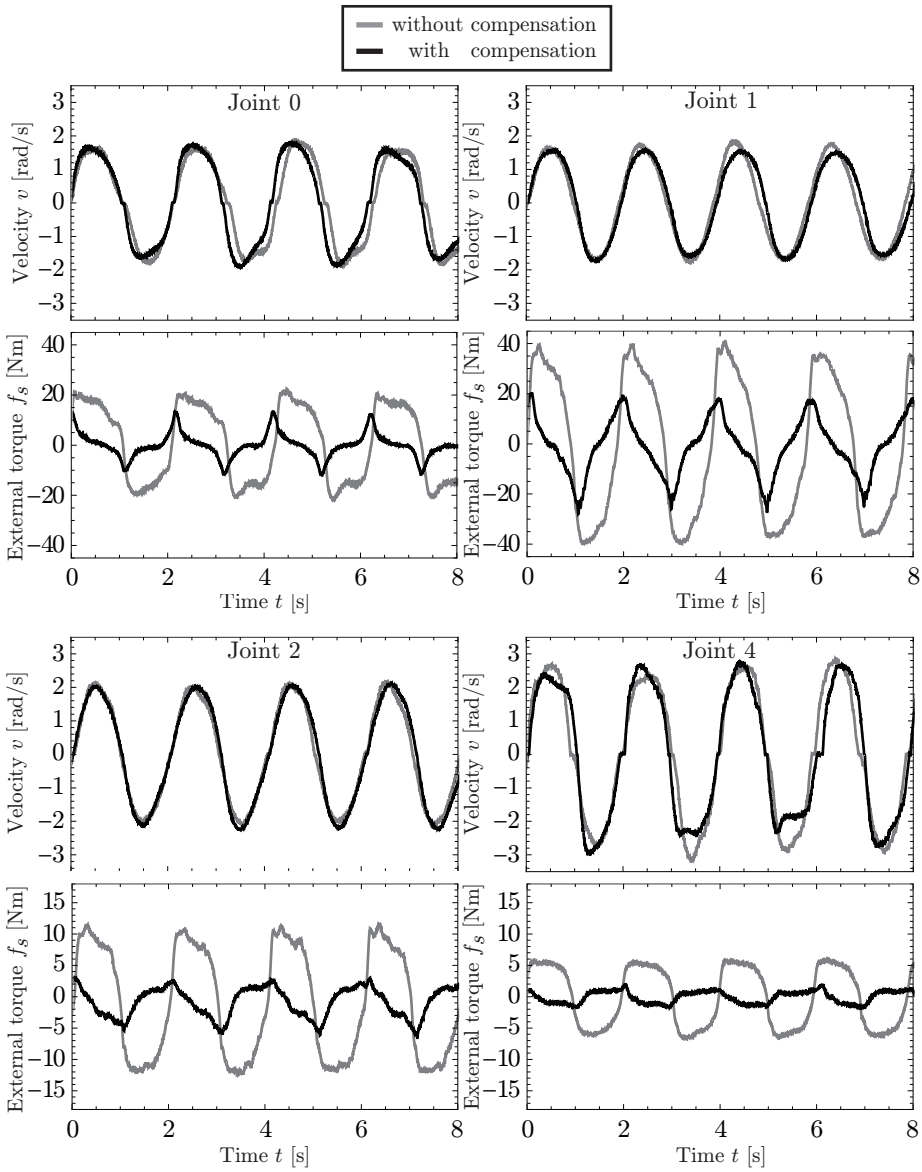

Figure 11: Experimental result of friction compensation. Data were not obtained from Joint 3 and 5 due to the limitation of the force sensor.

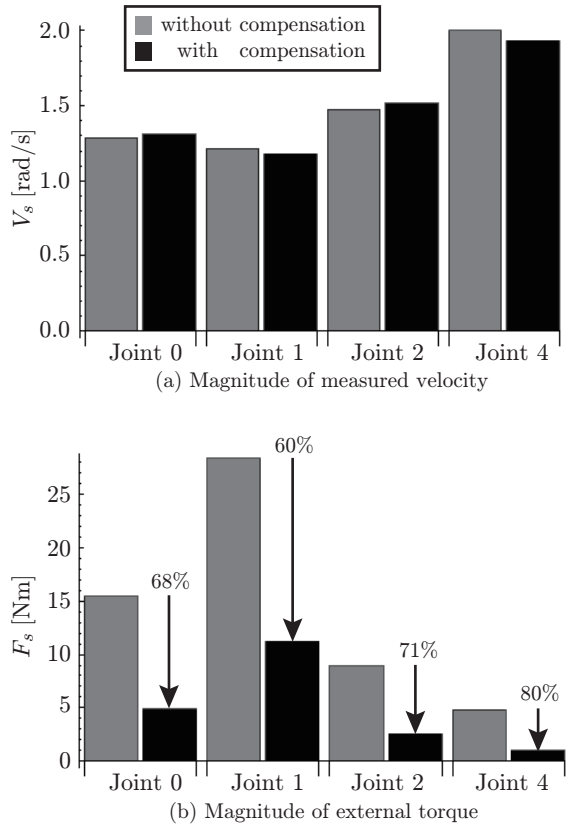

Figure 12: Average magnitudes (25) of measured velocity and external torque. Data were not obtained from Joint 3 and 5 due to the limitation of the force sensor.

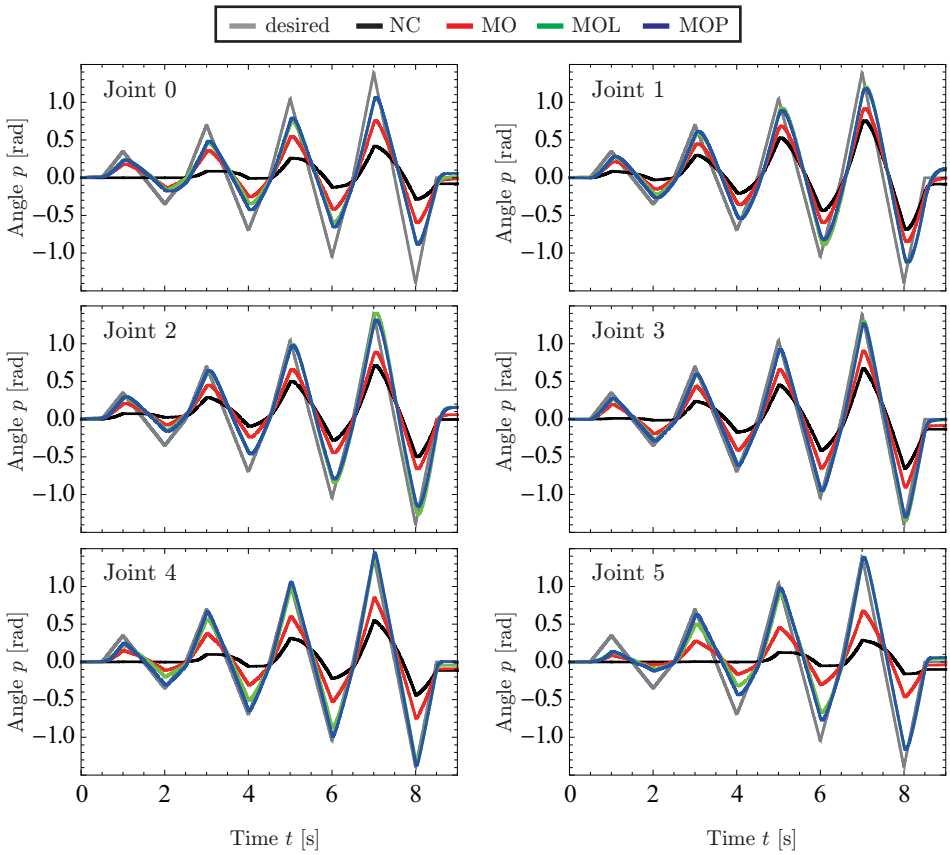

Figure 13: Experimental result of friction compensation in the four cases as follows: no compensation (NC), compensation by the model of Mahvash and Okamura [18] (MO), MO and linear viscosity compensation (MOL), MO and compensation using functions identified by the proposed procedure (MOP).

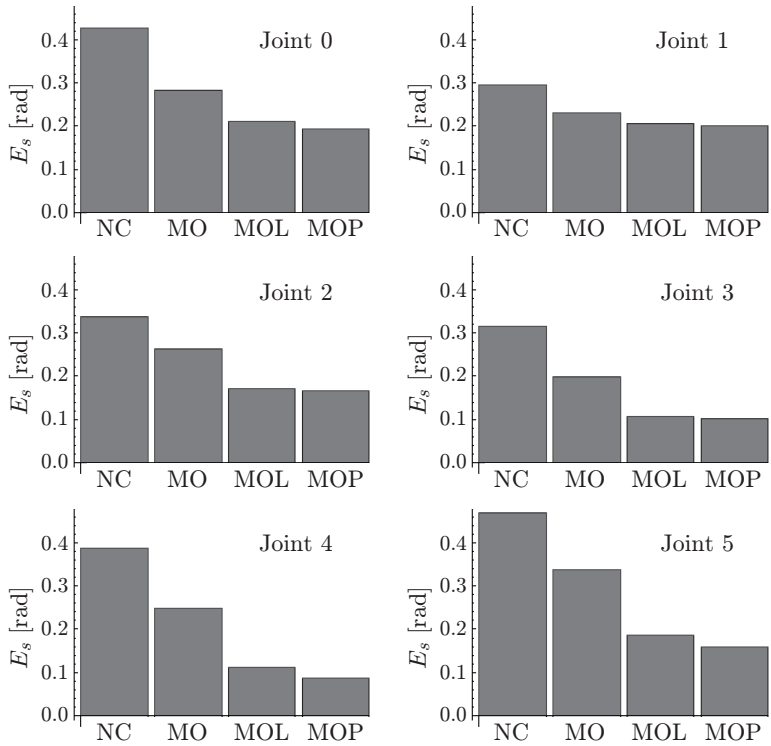

Figure 14: Average magnitudes (28) of measured position tracking error.